ChemPubSoc Europe

DOI: 10.1002/chem.201402616

CHEMISTRY
A European Journal
Full Paper

Photoinduced Electron Transfer

Geometric Influence on Intramolecular Photoinduced Electron Transfer in Platinum(II) Acetylide-Linked Donor–Acceptor Assemblies

Agustín Molina-Ontoria,[a] Danisha M. Rivera-Nazario,[a] Alexis Tigreros,[b] Alejandro Ortiz,[b] José E. Nuñez,[a] Braulio Insuasty,[b] Daniela Lueders,[c] Silke Wolfrum,[c] Dirk M. Guldi,*[c] and Luis Echegoyen*[a]

Abstract: A new donor–acceptor system, in which the electron donor triphenylamine (TPA) and the electron acceptor C_{60} are bridged through a *cis*- or *trans*-platinum(II) acetylide spacer have been prepared. Ground-state studies were conducted using electrochemistry and UV/Vis spectroscopy. Fluorescence studies suggested that charge transfer is the deactivation mechanism for the singlet excited state, and this was verified by transient absorption spectroscopy. Selective photoexcitation of **1** and **2** at 387 nm leads to a fast charge transfer between the TPA and C_{60}, which gives rise to a radical ion-pair state ($TPA^{\bullet+}$–Pt–$C_{60}^{\bullet-}$). Our results suggest that charge transfer is favored for the *cis* configuration while the presence of the *trans* configuration in the Pt^{II} diacetylide results in a longer-lived charge separated states.

Introduction

Considerable conceptual and experimental effort has been devoted to mimic the photoinduced electron-transfer processes that occur during the initial steps in photosynthetic systems.[1–4] The utilization of artificial D–A systems in optoelectronic devices requires efficient light harvesting and conversion into power, and equally efficient electron and hole-transport properties.[5,6] Upon illumination, the artificial D–A system must achieve efficient charge transfer leading to a long-lived charge separated state (D^{+}–A^{-}). To achieve this goal, careful design of the donor, the acceptor and the nature of the spacer that links the electroactive moieties is necessary.[7,8]

The optical and electronic properties of conjugated molecules undergo dramatic changes when a heavy atom is incorporated in the system. It is known that platinum acetylide complexes exhibit a large spin-orbit coupling (SOC) that facilitates a fast intersystem crossing from the singlet excited state to the triplet excited state.[9] Thus, platinum acetylide complexes are very promising candidates as donors for bulk-heterojunction (BHJ) solar cells,[10–15] exhibiting efficiencies up to 4.1%.[16] More recently, they have also been used in dye-sensitized solar cells (DSSC).[17–19] Furthermore, platinum acetylide complexes have been extensively used as organogelators,[20–23] in nonlinear optical applications, in electroluminescent devices[23–25] and as sensors.

Inclusion of the platinum atom in donor–bridge–acceptor (D–B–A) systems limits the conjugation, however some overlap of the platinum d orbitals and the alkyne π orbitals occurs which facilitates electronic delocalization.[26] Effective electron transfer through a platinum(II) diacetylide bridge was demonstrated in 2003 by Kushmerick et al. by measuring the conductance of a single molecule junction.[27] Later, Okada developed a D–*cis*-Pt–A system, which exhibited long lifetimes for the charge separated state (CS; 839 ns in toluene), thus minimizing the SOC effect.[28,29] These multicomponent systems σ-bonded to the Pt^{II} centers have been connected to different electron donors, such as porphyrins,[30] phthalocyanines[31] or bodipy[32] moieties resulting in efficient energy transfer processes. Triphenylamines are one of the most used moieties in D–B–A conjugated systems[33] because of their three-dimensional propeller structure, which is beneficial for improving solution processability, strong electron-donor properties and excellent hole-injection and transport properties via radical cation species. In addition, triphenylamines have been widely explored as active components for the preparation of high-performance dye-sensitized solar cells,[34–38] solution-processable small-molecule donors for bulk-heterojunction solar cells[39–41] and for light-emitting diodes (OLEDs).[42,43] It has been demonstrated that changing the nature of the acetylide ligand and the geometry

[a] *Dr. A. Molina-Ontoria, D. M. Rivera-Nazario, Prof. J. E. Nuñez, Prof. L. Echegoyen*
Department of Chemistry, University of Texas at El Paso
799618-0519 El Paso, Texas (USA)
E-mail: echegoyen@utep.edu

[b] *A. Tigreros, Prof. A. Ortiz, Prof. B. Insuasty*
Departamento de Química, Universidad del Valle, Cali, Colombia

[c] *D. Lueders, S. Wolfrum, Prof. D. M. Guldi*
Department of Chemistry and Pharmacy
Interdisciplinary Center for Molecular Materials (ICMM)
University of Erlangen-Nurenberg
Egerlandstrasse 3, 91058 Erlangen (Germany)
E-mail: dirk.guldi@chemie.uni-erlangen.de

Supporting information for this article is available on the WWW under http://dx.doi.org/10.1002/chem.201402616.

of the Pt^{II} complex can have a strong impact in the photophysical properties of similar compounds.[44,45] Based on these facts, in this study we report the synthesis and photophysical behavior of D–B–A conjugates in which D is a triphenylamine fragment, A is C_{60}, and B is a square-planar platinum linker, either *trans*-Pt or *cis*-Pt (Figure 1).

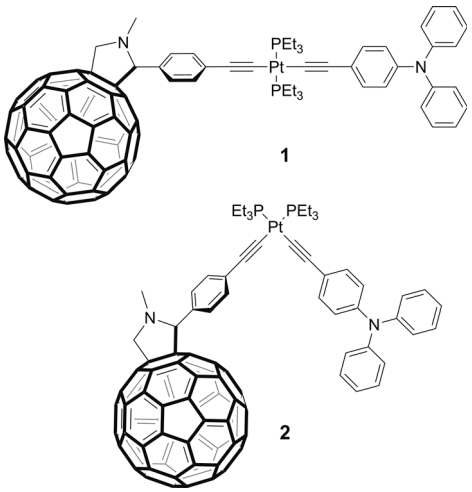

Figure 1. Structures of TPA–*trans*-Pt–C_{60} (**1**) and TPA–*cis*-Pt–C_{60} (**2**).

Results and Discussion

The synthetic pathway for the preparation of the σ-bonded Pt^{II} acetylide electron donor–acceptor conjugates **1** and **2** was conducted by stepwise approaches to obtain asymmetrically substituted derivatives, which involves the assembly of the 4-ethynyltriphenylamine with the corresponding Pt^{II} complexes (*trans* or *cis*) in the presence of catalytic amounts of CuI and diisopropylamine in THF. This was followed by a second catalyzed-dehydrohalogenation coupling reaction with 4-ethynylbenzaldehyde, to yield **6** and **7**. Finally, **1** and **2** were obtained in moderate yields as brown solids using 1,3-dipolar cycloaddition reactions of the corresponding azomethine ylides, generated in situ in toluene from sarcosine and aldehydes **6** or **7** (Scheme 1).

We also synthetized compounds **10** and **11** as references for the electrochemical studies to shed light on the electronic interaction between the donor and the acceptor. The synthesis was performed by assembling the 4-ethynylbenzaldehyde with the corresponding *trans*- or *cis*-Pt^{II} complexes, followed by 1,3-dipolar cycloadditions with C_{60}, to obtain **10** and **11**.

Complete structural characterization of **1**, **2** and the corresponding intermediates and the reference compounds was accomplished using spectroscopic techniques such as ^{1}H NMR, ^{31}P NMR, IR, UV/Vis spectroscopy, and mass spectrometry (MALDI-TOF). The ^{1}H NMR and ^{13}C NMR spectra reveal the expected resonance signals of the aliphatic and aromatic protons and carbons. The ^{31}P NMR displayed sharp singlets at 11.8 and

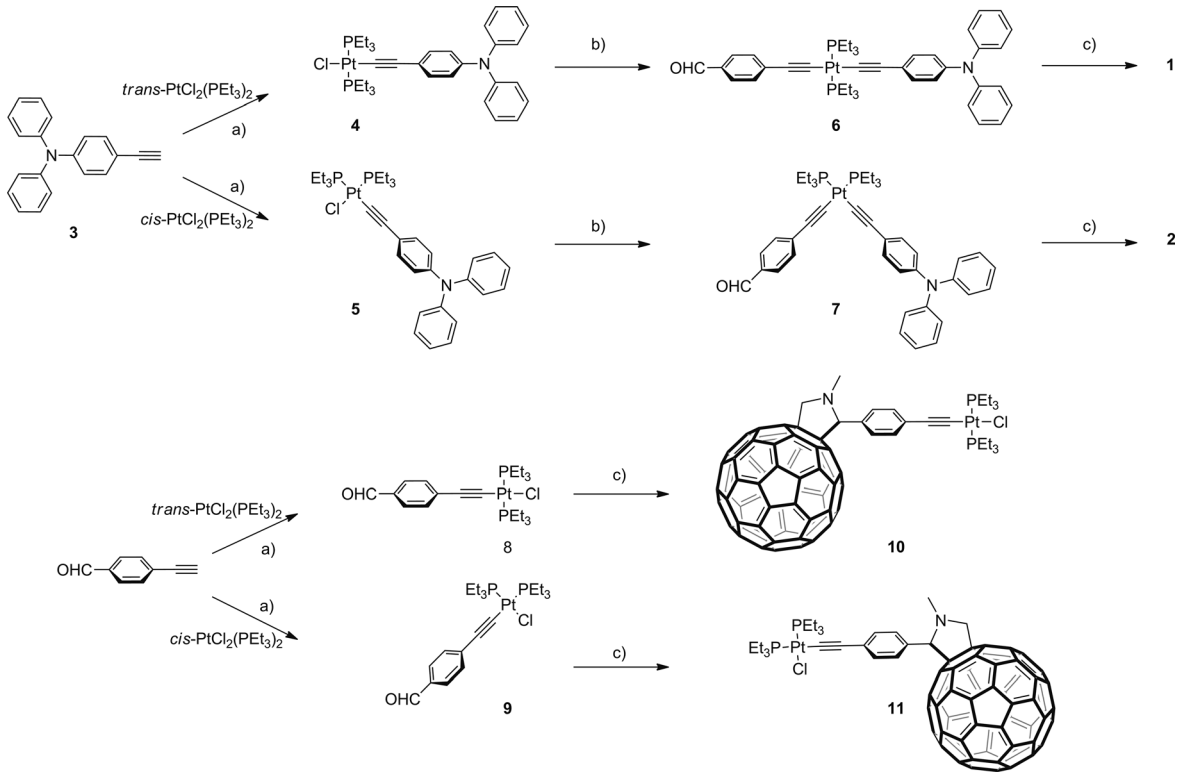

Scheme 1. Synthesis of **1** and **2**. Reagents and conditions: a) **3**, *trans*-$PtCl_2(PEt_3)_2$ or *cis*-$PtCl_2(PEt_3)_2$, CuI, THF, iPr_2NH, reflux, 7 h, $y = 47$ and 52%, respectively; b) 4-ethynylbenzaldehyde, CuI, THF, NEt_3, reflux, 7 h, $y = 66$–71%; c) **6** or **7**, C_{60}, sarcosine, chlorobenzene, reflux, 5 h, $y = 32$–35%.

11.7 ppm for **1** and **2**, respectively, which were slightly shifted upfield relative to the starting platinum compounds **6** and **7** (for more details see the Supporting Information). The presence of C_{60} was also confirmed by FTIR spectra, showing the characteristic frequency at 525 cm^{-1} and those of the alkynes around 2100 cm^{-1}, while the carbonyl peak appeared at 1700 cm^{-1} for the precursors. In addition, the presence of **1** and **2** were corroborated by MALDI-TOF mass spectrometry, which clearly showed the molecular ion peak $[M]^+$ at 1575 *m*/*z*.

The geometrical optimizations and the ground electronic states of complexes **1** and **2** were simulated by density functional theory (DFT) using Gaussian 09 (see the Supporting Information). The specific DFT methods used include Becke's exchange (B3) functional, in conjunction with the Lee–Yang–Parr (LYP) correlation functional, commonly known as the B3LYP method. The basis set used in all calculations was LANL2DZ, an effective core potential (ECO) basis set that was used to provide some corrections for the scalar relativistic effects of the Pt atom.[46]

The results of the structural optimizations for complexes **1** and **2** showed, as expected, a well-defined difference in the geometrical distributions of the ligands linked to the platinum core, with angles between the phenyl rings attached to the metal of 179.2° in **1** and 85.1° in **2**. There is a notable change in the distance between the nitrogen of the triphenylamine group and the fullerene moiety going from the *trans* isomer (18.1 Å) to the *cis* isomer (12.1 Å), which could play an important role in the electron transfer properties (Figure 2).

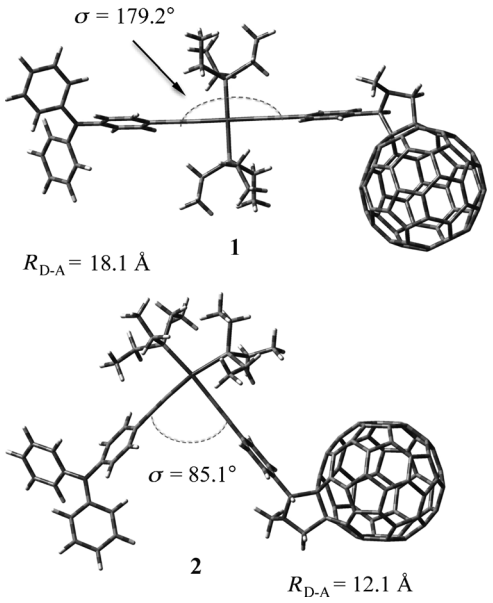

Figure 2. Geometries optimization at DFT-B3LYP-LanL2DZ level of **1** and **2**.

The results of the ground state electronic structure calculations were used to generate the frontier molecular orbital (FMO) electron density of the two highest occupied molecular orbitals (HOMO and HOMO−1) and of the two lowest unoccupied molecular orbitals (LUMO and LUMO+1) as shown in Figure 3. In general, the electron density of the HOMO includes contributions mainly from the triphenylamine unit with a small contribution from the platinum d orbitals, whereas the density of the HOMO−1 includes contributions from the platinum and the aryleneethynylene ligands. These results reveal some conjugation between the triphenylamine and the platinum acetylide groups. On the other hand, their LUMO and LUMO+1 densities are located exclusively on the fullerene C_{60} moiety, due to the high acceptor capability of the latter. There is no isomeric influence in the topology of the FMOs. In contrast, the energy levels were somewhat affected when going from the *trans* to the *cis* geometry (Table S1 in the Supporting Information).

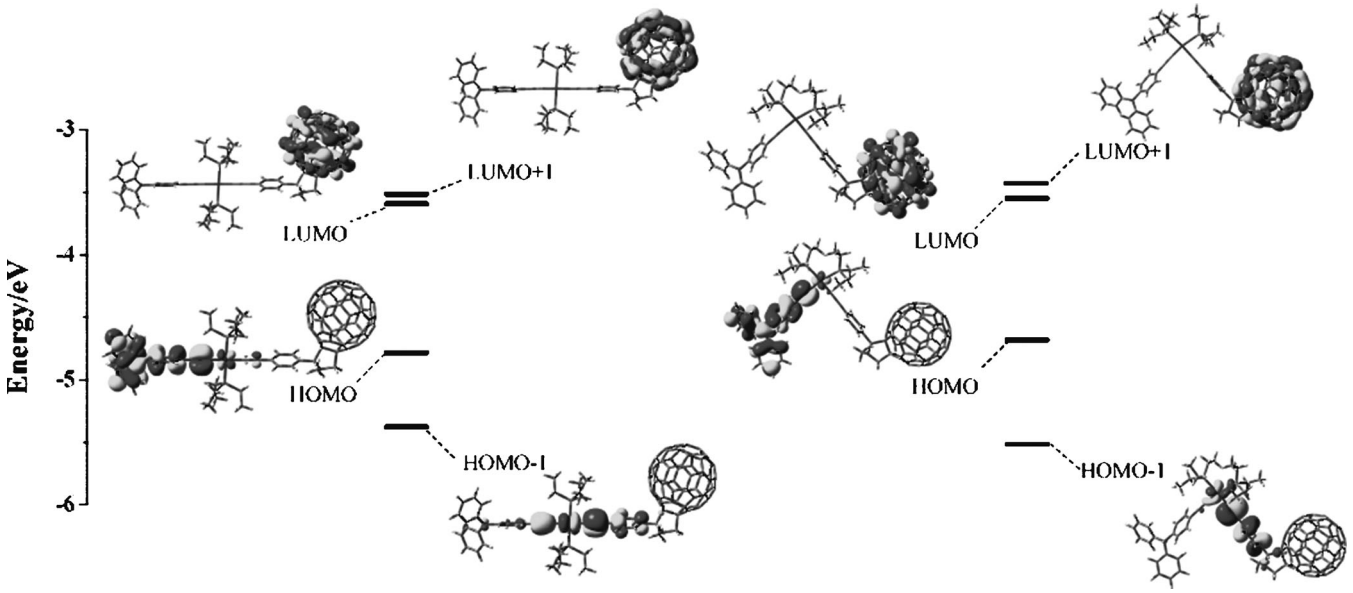

Figure 3. Molecular orbital calculations at DFT-B3LYP-LanL2DZ level of **1** and **2**.

The optical properties of compounds **1** and **2** were analyzed by ultraviolet–visible absorption. Figure 4 shows the optical absorption spectra of the *trans*-TPA–Pt–C_{60} (**1**) and for the reference compounds such as 4-ethynyltriphenylamine (**3**), compound **6**, and **4** in diluted dichloromethane solutions (optical absorption spectrum of **2**, Figure S1 in the Supporting information). The assembly of the triphenylamine with the platinum (**4** and **5**) displayed red-shifted absorptions centered at 350 nm, and a shoulder at 312 nm with respect to the 4-ethynyltriphenylamine (329 nm). Interestingly, increasing the overall length by assembling the 4-ethynylbenzaldehyde in **6** and **7**, results in an intramolecular push–pull effect and therefore, bathocromically shifted absorptions were observed, at 366 and 362 nm, respectively, due to the weak electron-withdrawing effect of the aldehyde, accompanied by an increase of the extinction coefficient. The latter suggests that the π-conjugation through the platinum(II) is limited, but intact. For the D–B–A systems **1** and **2**, the characteristic absorptions of the C_{60} moiety appear at 430 nm and in the UV–visible region (250–340 nm) which are partially masked by the stronger absorption of the triphenylamine unit. The absorption properties of the *trans* configuration are similar to those of the *cis*; for example, both exhibit a broader and blue-shifted maxima with respect to precursors **6** and **7**, due to the insertion of the C_{60} at 356 and 354 nm, respectively. Slightly lowered band-gaps were obtained for **1** and **2** (0.3 eV) relative to the pure donor 4-ethynyltriphenylamine (**3**), which is indicative of weak electronic interactions between the electroactive moieties in the ground state.[16]

Electrochemical studies were conducted to probe the electronic coupling between the donor and the acceptor in the ground state. The electrochemistry of TPA–Pt–C_{60} conjugates **1** and **2** was studied by cyclic voltammetry (CV) and differential pulse voltammetry (DPV) in 0.1 M $TBAPF_6/CH_2Cl_2$ at a scan rate of 100 mV s^{-1}. Table 1 summarizes the redox potentials for **1** and **2** along with those for their respective reference compounds. Figure 5 shows the CVs for **1**, **6**, **2**, and **7**. The cyclic voltammograms of **1** and **2** reveal three one-electron reversible reductions corresponding to C_{60} centered processes. On the oxidative scan, two oxidation processes were observed for **1**, which correspond to the triphenylamine donor (reversible) and to the platinum bridge (irreversible) at +0.24 and +0.84 V, respectively. The second oxidation potential is tentatively assigned to a two-electron oxidation process arising from the platinum bridge and the triphenylamine moiety.

The same observation was made for **2**, with two oxidations at +0.28 (reversible) and +0.88 V (irreversible). Again, the second oxidation is tentatively assigned to a two-electron process. The presence of the platinum atom in **6** and **7** produces a noteworthy cathodic shift of more than 300 mV for the TPA moiety when compared to **3**. The latter suggests that the platinum bridge increases the TPA electron-donating ability and that a strong binding with the metal center occurs. Similarly, the first reduction of **1** and **2** are cathodically shifted 90 and

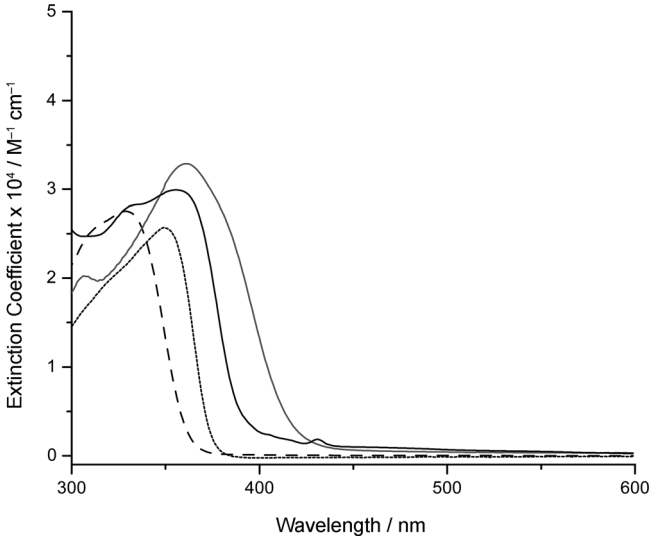

Figure 4. Room temperature absorption spectra of **1** (solid line) and reference compounds 4-ethynyltriphenylamine (dashed line), **4** (dotted line) and **6** (solid grey line) in dichloromethane solutions.

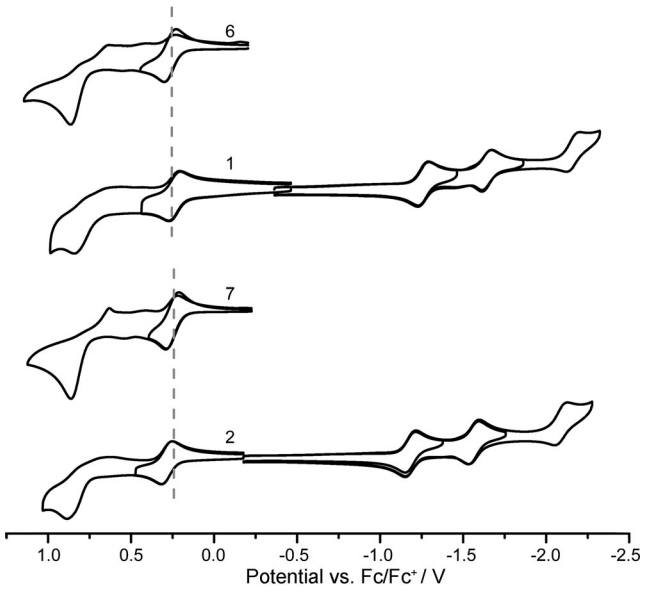

Figure 5. Cyclic voltammogram of *trans*- (**1**) and *cis*-TPA–Pt–C_{60} (**2**) conjugates and their corresponding reference compounds in $TBAPF_6/CH_2Cl_2$ at a scan rate of 100 mV s^{-1}.

Table 1. Electrochemical data of *trans*- (**1**) and *cis*-TPA–C_{60} (**2**) electron donor–acceptor conjugates and their corresponding references.

Compound	E^1_{ox}	E^2_{ox}	E^1_{red}	E^2_{red}	E^3_{red}
3	+0.58				
1	+0.24	+0.84	−1.26	−1.65	−2.16
4	+0.28	+0.90			
6	+0.27	+0.87			
10	+0.80	–	−1.17	−1.56	−2.08
2	+0.28	+0.88	−1.19	−1.56	−2.09
5	+0.32	+0.95			
7	+0.25	+0.86			
11	+0.87	–	−1.16	−1.55	−2.07

30 mV, respectively, when compared to the reference compounds (**10** and **11**). The latter observation corroborates that electronic interaction in the ground state is occurring through the platinum metal center in which the *trans* geometry is favored. In line with steady state absorption studies, the electrochemical studies confirm that the band-gap is narrower for **1** and **2** relative to **10** and **11**, which is a clear indication of significant interactions between the donor and the acceptor in the ground state.

In order to obtain further insights into the nature of the interactions between the TPA and the C_{60} in the excited state, emission and transient absorption measurements of **1** and **2** with respect to their reference compounds were performed in toluene (Figure S2 in the Supporting Information). To this end, we measured the fluorescence upon excitation at 350 nm under deoxygenated conditions as shown in Figure 6. For **6** and **7**, we observed an emission maximum at 419 and 505 nm in both cases.

The former emission arises from $^1\pi$–π^*, while the latter is attributed to a phosphoresce phenomenon from $^3\pi$–π^*, which is essentially located on the TPA.[47] The fluorescence quantum yields are 2.06×10^{-3} for **6** and 1.42×10^{-3} for **7**. No significant effects were observed when increasing the polarity of the solvent (THF).

Inspecting the fluorescence features of the TPA in the D–B–A (**1** and **2**) systems provides the first indication about the deactivation mechanism of the excited state. Upon excitation at 350 nm, the TPA fluorescence is strongly quenched ($\Phi = 5.1\times10^{-5}$ for **1** and $\Phi = 4.4\times10^{-5}$ for **2**) which indicates that the excited-state interactions between the electron-donating TPA and the electron-accepting C_{60} are significantly strong. In addition, increasing the solvent polarity results in a rather strong quenching of the TPA fluorescence ($\Phi = 4.4\times10^{-5}$ for **1** and $\Phi = 3.7\times10^{-5}$ for **2**), which suggests a charge-transfer process as a deactivation pathway (Figure 6). In line with these results, the *cis* configuration results in a stronger TPA fluorescence quenching when compared with that of the *trans* configuration, which implies stronger interactions between the electroactive moieties in the excited state, possibly as a result of a shorter through-space distance between the TPA and C_{60} moieties.

Further spectroscopic evidence of the deactivation processes evolving from the excited states by means of charge-transfer and/or energy-transfer mechanism, were obtained from complementary transient absorption measurements. In pump-probe experiments with references **6** and **7**, we note the immediate formation of a transient spectrum, which exhibits maxima at 590, 690, 800, and 1025 nm (Figure 7). These features correspond to the singlet excited state of either **6** or **7** in, for example, THF or benzonitrile. As time progresses, the latter transients turned out to be short-lived, owing to the fact that they are transformed with lifetimes of 200(±10) and 230(±10) ps for **6** and **7**, respectively, into the corresponding triplet excited states via intersystem crossing. The new features, which correspond to the triplet excited state, appear at 555 nm as a shoulder and 600, 800, and 915 nm maxima.

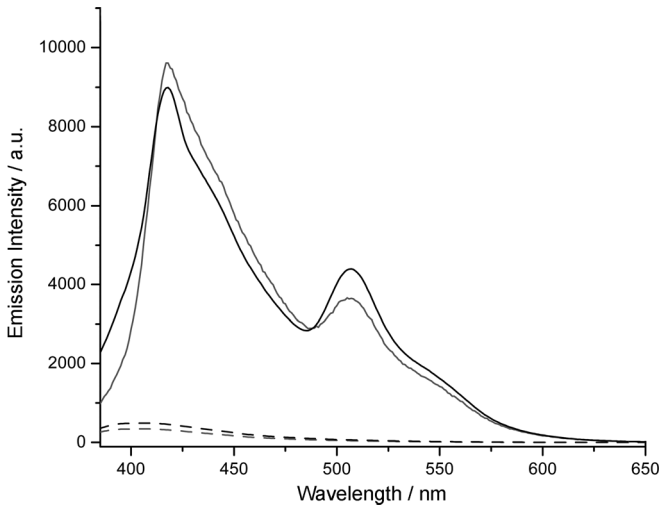

Figure 6. Room temperature fluorescence spectra of **1** (dashed line) and **2** (grey dashed line) and reference derivatives **6** (solid line) and **7** (grey solid line) in THF after photoexcitation at 350 nm.

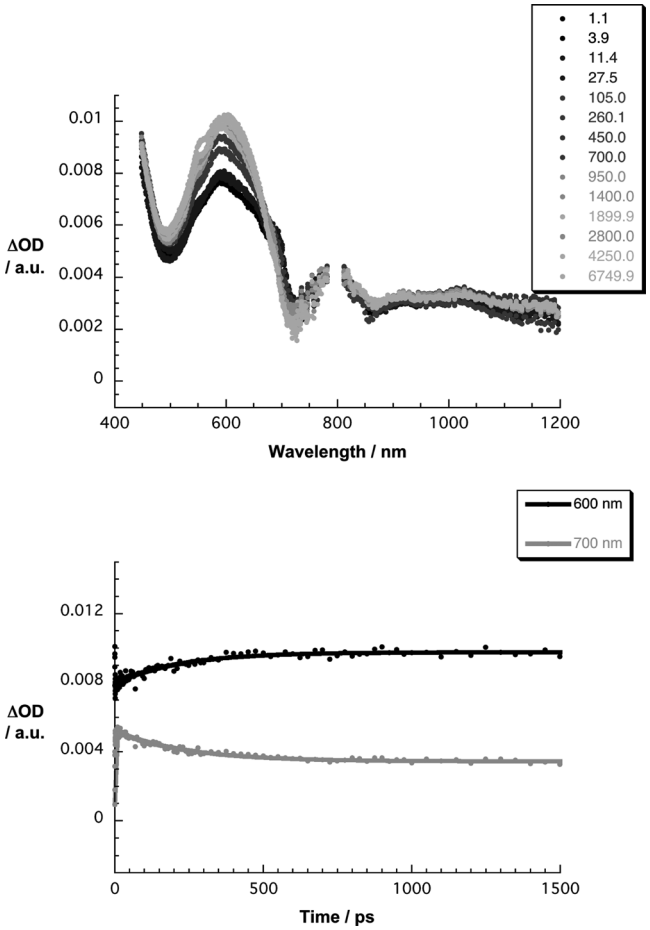

Figure 7. Upper plot: differential absorption spectra (visible and near-infrared) obtained with femtosecond pump-probe experiments (387 nm) of **7** (10^{-5} M) in benzonitrile with time delays between 0.1 and 6749.9 ps at room temperature. Lower plot: time absorption profiles of the spectra shown in the upper part at 600 (black spectrum) and 700 nm (grey spectrum) monitoring the excited-state decay.

For electron D–B–A conjugates **1** and **2**, photoexcitation at 387 nm leads to an instantaneous development of transient features that resemble those seen for reference **6** and **7** (see Figure 8 and Figure S3 in the Supporting Information). In particular, the singlet excited state markers at 590, 690, 800, and 1025 nm are discernable throughout the visible and near-infrared range. However, instead of intersystem crossing with 200(±10) ps for **6** and 230(±10) ps and **7**, a much faster excited-state deactivation occurs in the presence of C_{60}. In THF, for example, multiwavelength analyses indicate lifetimes of 3.3(±0.5) ps for **1** and 1.9(±0.5) ps for **2**. In benzonitrile, a marked acceleration with lifetimes of 2.0(±0.5) ps for **1** and 1.6(±0.5) ps for **2** evolves. The product of these decays is a transient species that has nothing in common with the triplet excited state of **6** and **7**, neither with the C_{60} singlet nor triplet excited state. Instead, new features in the visible and in the near-infrared evolve that include maxima at 460, 790 and 1010 nm, respectively.

Pulse radiolytic oxidation of **3** (Figure 9) and reduction of C_{60} induces transient maxima at 750 and 1010 nm, respectively. Considering the aforementioned in concert, we reach the conclusion that 387 nm excitation of **1** and **2** in THF and benzonitrile leads to charge separation that is mediated through the central Pt linker and gives rise to the formation of the $TPA^{\bullet+}$–Pt–$C_{60}^{\bullet-}$ radical ion pair states. Apparently, the *cis* configuration favors charge separation relative to the *trans* configuration. In addition, charge recombination shows a similar trend. In particular, the $TPA^{\bullet+}$–Pt–$C_{60}^{\bullet-}$ radical ion pair state decays in **1** with a lifetime of 95(±5) ps, while for **2** the corresponding lifetime is 64(±5) ps in THF. It is important to mention that the electrochemical measurements suggest similar driving forces for charge separation (~1.0 eV) as well as charge recombination (~1.48 eV) for **1** and **2**, respectively. Considering the fact that the product of charge recombination is the ground state rather than a low lying C_{60} triplet excited state (1.5 eV) it is interesting to note that the more polar benzonitrile slows down the process. In this solvent, lifetimes of 103(±5) ps for **1** and of 89(±5) ps for **2** were determined. In other words, charge recombination, despite the large driving force, is located in the normal region of the Marcus parabola. This finding correlates with the inherent instability of the one electron oxidized TPA, which is known to dimerize.

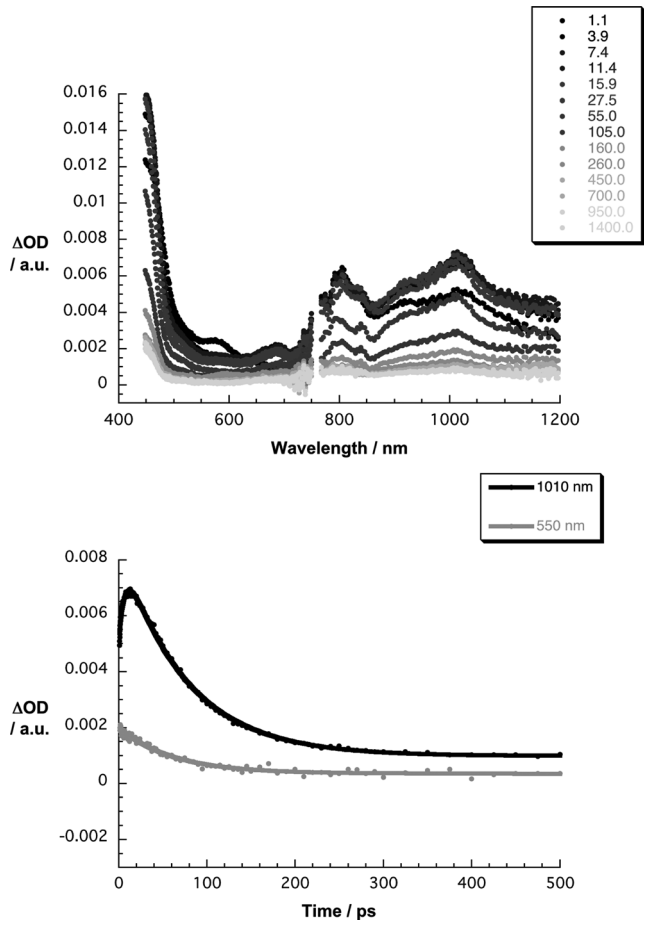

Figure 8. Upper plot: differential absorption spectra (visible and near-infrared) obtained with femtosecond pump-probe experiments (387 nm) of **2** (10^{-5} M) in benzonitrile with time delays between 0.1 and 1400.0 ps at room temperature. Lower plot: time absorption profiles of the spectra shown in the upper part at 550 (grey spectrum) and 1010 nm (black spectrum) monitoring the charge separation and charge recombination.

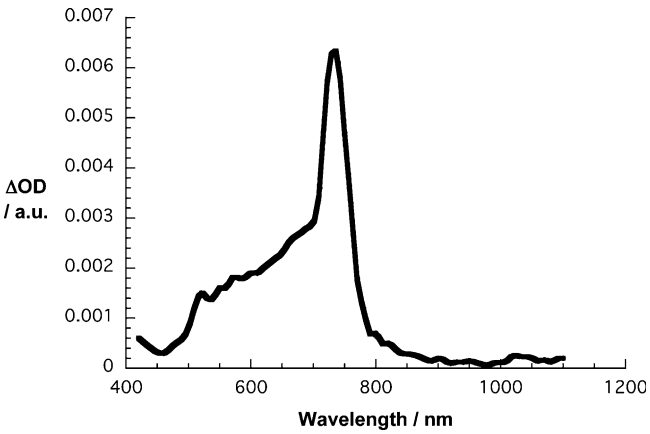

Figure 9. Differential absorption spectrum (visible and near-infrared) obtained upon pulse radiolytic oxidation of **3** (10^{-5} M) in aerated dichloromethane with a time delay of 100 μs at room temperature.

Conclusion

In summary, we have carried out the syntheses of new donor–acceptor systems which, assembled through a *trans*-platinum(II) or *cis*-platinum(II), undergo photoinduced electron transfer. The electrochemical analysis reveal significant interactions between the TPA and the C_{60} in the steady state. It is known that a change in the geometry of the Pt^{II} has a strong impact in the photophysical properties, this approach allows the efficient formation of the radical ion pair state $TPA^{\bullet+}$–Pt–$C_{60}^{\bullet-}$ upon photoexcitation of the TPA at 350 nm. Besides the rather close proximity of the electroactive units in the *cis* assembly (12.1 Å for *cis* and 18.1 Å for *trans*), the electron transfer takes place through the central Pt linker, which is faster for the *cis* with respect to the *trans* configuration. On the other hand, longer lifetimes for the charge separated states were ob-

tained for the *trans* geometry, 95 and 103 ns in THF and benzonitrile, respectively, placing the charge transfer process in the normal region of the Marcus parabola.

Experimental Section

Reagents were used as purchased. All solvents were dried according to standard procedures. All air-sensitive reactions were conducted under an argon atmosphere. FTIR spectra were recorded using a Bruker Tensor 27 spectrometer with neat samples. Absorption studies were performed using a Cary 5000 UV/Vis/NIR spectrometer from Varian using fused Quartz glass cuvettes with a 1 cm optical path. Fluorescence measurements were performed in a JABSCO spectrofluorometer (FP-8500). NMR spectra were recorded on a 600 MHz JEOL (^{1}H: 600 MHz, ^{13}C: 125 MHz) spectrometer at 298 K using partially deuterated solvents as internal standards. Coupling constants (J) are reported in Hz and chemical shifts (δ) in ppm. Multiplicities are denoted as follows: s = singlet, d = doublet, t = triplet, m = multiplet, dt = double triplet. Matrix assisted laser desorption ionization (coupled to a time-of-flight analyzer) experiments (MALDI-TOF) were recorded on a Bruker microFLEX spectrometer. Flash chromatography was performed using silica gel (Sorbent technologies 60, 230–400 mesh). Analytical thin layer chromatography (TLC) was performed using aluminum coated Sorbent technologies 60 UV254 plates. Compounds **3**, **8**, and **9**, were prepared according to previously reported synthetic procedures.

Electrochemical studies of TPA—Pt–fullerene dyads

These experiments were performed in anhydrous dichloromethane (DCM, Sigma–Aldrich, anhydrous, 99%). Tetrabutylammonium hexafluorophosphate ($TBAPF_6$, Aldrich, 98%) was added as the supporting electrolyte and used after recrystallization from ethanol. Cyclic voltammetry (CV) and differential pulse voltammetry (DPV) experiments were performed under an argon atmosphere at room temperature using a CH Instrument potentiostat. The scan rate for CV experiments was 100 mV s^{-1}. For DPV experiments, a scan rate of 100 mV s^{-1} and a pulse rate of 0.5 s with increments of 4 mV and amplitude of 50 mV were used. A standard three-electrode set up consisting of a glassy carbon working electrode (1.0 mm), a platinum wire as counter electrode (Aldrich, 1.0 mm) and a silver wire as pseudoreference electrode (Aldrich, 1.0 mm) was used. The redox couple ferrocene/ferrocenium (Fc/Fc^+) was used as internal reference to measure the potentials. The half-wave potentials ($E_{1/2}$) were determined from CV experiments as $(E_{pa}+E_{pc})/2$, where E_{pa} and E_{pc} are the anodic and cathodic peak potentials, respectively.

General procedure for the synthesis of 4 and 5

A solution of 4-ethynyltriphenylamine (0.35 mmol), CuI (5 mg), and the corresponding *trans*-$PtCl_2(PEt_3)_2$ or *cis*-$PtCl_2(PEt_3)_2$ (200 mg, 0.40 mmol) in THF (15 mL) and diisopropylamine (2 mL) was stirred under argon for 6 h at 50 °C. After evaporation of the solvent, the crude was purified by flash column chromatography on SiO_2 using CH_2Cl_2 as eluent. Finally, the products were dried at 40 °C under vacuum, affording **4** and **5** as white solids.

Compound 4: Yield 52%; ^{1}H NMR ($CDCl_3$, 600 MHz): δ = 7.22–7.20 (m, 4H, aromatic-H), 7.11 (d, 2H, J = 8.2 Hz, aromatic-H), 7.06–7.04 (m, 4H), 6.98 (dd, 2H, J = 8.2 Hz, J = 1.6 Hz, aromatic-H), 6.92 (d, 2H, J = 8.2 Hz, aromatic-H), 2.08–2.03 (m, 12H, -CH_2- PCH_2CH_3), 1.21–1.16 ppm (m, 18H, -CH_3, PCH_2CH_3); ^{13}C NMR ($CDCl_3$, 150 MHz): δ = 147.7, 145.6, 131.6, 129.4, 124.1, 123.8, 122.6, 14.5, 8.1 ppm; ^{31}P NMR (243 MHz, $CDCl_3$): δ = 15.3 ppm (t, $J_{Pt,P}$ = 2345.0 Hz); FTIR (neat): $\tilde{\nu}$ = 3031, 2929 (C–H), 2120 (alkyne), 1588, 1500, 1311, 1033, 824, 693 cm^{-1}; UV/Vis (CH_2Cl_2), λ_{max} (ε): 350 nm (25800 mol^{-1} dm^3 cm^{-1}); MALDI-TOF m/z: 735.7 [M^+].

Compound 5: Yield 48%; ^{1}H NMR ($CDCl_3$, 600 MHz): δ = 7.23–7.20 (m, 4H, aromatic-H), 7.11 (d, 2H, J = 8.2 Hz, aromatic-H), 7.07–7.05 (m, 4H), 6.98 (dt, 2H, J = 8.2 Hz, J = 1.6 Hz, aromatic-H), 6.92 (d, 2H, J = 8.2 Hz, aromatic-H), 2.08–2.03 (m, 12H, -CH_2- PCH_2CH_3), 1.21–1.16 ppm (m, 18H, -CH_3, PCH_2CH_3); ^{13}C NMR ($CDCl_3$, 150 MHz): δ = 147.7, 145.2, 131.7, 129.1, 124.7, 124.1, 123.9, 123.1, 122.6, 101.3, 14.5, 8.1 ppm; ^{31}P NMR (243 MHz, $CDCl_3$): δ = 15.4 ppm (t, $J_{Pt,P}$ = 2345.0 Hz); FTIR (neat): $\tilde{\nu}$ = 3029, 2964 (C–H), 2122 (alkyne), 1588, 1491, 1311, 1032, 823, 693 cm^{-1}; UV/Vis (CH_2Cl_2): λ_{max} (ε): 349 nm (24900 mol^{-1} dm^3 cm^{-1}); MALDI-TOF m/z: 735.7 [M^+].

General procedure for the synthesis of 6 and 7

A solution of 4-ethynylbenzaldehyde (0.35 mmol), CuI (5 mg), and the corresponding *trans*-Cl–Pt–TPA (**4**) or *cis*-Cl–Pt–TPA (**5**; 0.30 mmol) in THF (15 mL) and triethylamine (1 mL) was stirred under argon for 3 h at 50 °C. After evaporation of the solvent, the crude was purified by flash column chromatography on SiO_2 using CH_2Cl_2 as eluent. Finally, the products were dried at 40 °C under vacuum, affording **6** and **7** as yellow solids.

Compound 6: Yield 47%; ^{1}H NMR ($CDCl_3$, 600 MHz): δ = 9.91 (s, 1H, -CHO), 7.71 (d, 2H, J = 8.2 Hz, aromatic-H), 7.36 (d, 2H, J = 8.2 Hz, aromatic-H), 7.23–7.20 (m, 4H, TPA), 7.15 (d, 2H, J = 8.2 Hz, TPA), 7.07–7.05 (m, 4H, TPA), 6.99–6.96 (m, 2H, TPA), 6.93 (d, 2H, J = 8.2 Hz, TPA), 2.20–2.14 (m, 12H, -CH_2-, PCH_2CH_3), 1.25–1.29 ppm (m, 18H, -CH_3, PCH_2CH_3); ^{13}C NMR ($CDCl_3$, 150 MHz): δ = 191.7, 147.9, 145.2, 135.7, 132.9, 131.8, 131.3, 129.7, 129.4, 124.1, 124.0, 122.6, 117.3, 110.0, 109.7, 16.6, 16.5, 16.4, 8.5 ppm; ^{31}P NMR (243 MHz, $CDCl_3$): δ = 11.8 ppm (t, $J_{Pt,P}$ = 2345.0 Hz); FTIR (neat): $\tilde{\nu}$ = 2966, 2934 (C–H), 2097 (alkyne), 1693 (C=O), 1590, 1492, 1275, 1208, 1158, 1033, 836, 770, 693, 616, 525 cm^{-1}; UV/Vis (CH_2Cl_2): λ_{max} (ε): 366 (32900), 307 nm (20200 mol^{-1} dm^3 cm^{-1}); MALDI-TOF m/z: 828.2 [M^+].

Compound 7: Yield 52%; ^{1}H NMR ($CDCl_3$, 600 MHz): δ = 9.91 (s, 1H, -CHO), 7.70 (d, 2H, J = 8.2 Hz, aromatic-H), 7.35 (d, 2H, J = 8.2 Hz, aromatic-H), 7.22–7.20 (m, 4H, TPA), 7.14 (d, 2H, J = 8.2 Hz, TPA), 7.06–7.04 (m, 4H, TPA), 6.98–6.96 (m, 2H, TPA), 6.92 (d, 2H, J = 8.2 Hz, TPA), 2.18–2.13 (m, 12H, -CH_2-, PCH_2CH_3), 1.23–1.28 ppm (m, 18H, CH_3-, PCH_2CH_3); ^{13}C NMR ($CDCl_3$, 150 MHz): δ = 191.5, 147.8, 145.2, 135.2, 132.9, 131.81, 131.3, 129.7, 129.2, 124.1, 124.0, 122.6, 117.4, 110.1, 109.9, 16.4, 8.4 ppm; ^{31}P NMR (243 MHz, $CDCl_3$): δ = 11.7 ppm (t, $J_{Pt,P}$ = 2290.0 Hz); FTIR (neat): $\tilde{\nu}$ = 2966, 2934 (C–H), 2097 (alkyne), 1693 (C=O), 1590, 1552, 1492, 1453, 1275, 1208, 1158, 1012, 830, 770, 693, 616, 527 cm^{-1}; UV/Vis (CH_2Cl_2): λ_{max} (ε): 360 (28670), 306 nm (18700 mol^{-1} dm^3 cm^{-1}); MALDI-TOF m/z: 828.2 [M^+].

General procedure for the 1,3-dipolar cycloaddition reaction

The corresponding aldehyde (1 equiv), [60]fullerene (1.3 equiv) and sarcosine (5 equiv) were dissolved in chlorobenzene and the mixture was refluxed for 5 h. The reaction mixture was allowed to reach room temperature and the solvent was removed under vacuum. The crude was purified by flash column chromatography on SiO_2. The eluents are specified in each case. The black solids obtained were further purified by repeated (3×) precipitation and centrifugation in methanol to yield the corresponding hybrids as black solids.

Compound 10: First CS_2 was used as eluent in order to remove unreacted C_{60} and then toluene, 26% yield. ^{1}H NMR ($CDCl_3$, 600 MHz): $\delta = 7.62$ (br, 2H, aromatic-H), 7.28 (d, 2H, $J = 8.2$ Hz, aromatic-H), 4.96 (d, 1H, $J = 9.2$ Hz, CH_2 pyrrolidine), 4.86 (d, 1H, $J = 9.2$ Hz, CH pyrrolidine), 4.22 (s, 1H, CH_2 pyrrolidine), 2.77 (s, 3H, aliphatic-CH_3), 2.09–2.03 (m, 12H, aliphatic -CH_2-), 1.21–1.15 ppm (m, 18H, aliphatic -CH_3); ^{13}C NMR ($CDCl_3$, 150 MHz): $\delta = 156.4$, 153.6, 153.5, 147.3, 146.9, 146.6, 146.50, 146.2, 146.0, 145.6, 145.5, 145.3, 144.8, 144.7, 144.4, 143.2, 143.0, 142.7, 142.6(3), 142.3(2), 142.2(2), 142.1(3), 142.0, 141.9, 141.7, 141.6, 139.9, 139.7, 136.9, 136.6, 135.8, 133.9, 131.2, 129.1, 101.3, 100.3, 83.6, 70.2, 69.0, 40.3, 14.6(2), 14.4, 8.2(2) ppm; ^{31}P NMR (243 MHz, $CDCl_3$): $\delta = 15.4$ ppm (t, $J_{Pt,P} = 2383.0$ Hz); FTIR (neat): $\tilde{\nu} = 2966$, 2934 (C–H), 2097 (alkyne), 1590, 1552, 1492, 1453, 1275, 1208, 1158, 1012, 830, 770, 693, 616, 527 cm^{-1}; FTIR (neat) $\tilde{\nu} = 2962$, 2776 (C–H), 2210 (alkyne), 1589, 1493, 1311, 1034, 863, 696, 523 cm^{-1}; UV/Vis (CH_2Cl_2): λ_{max} (ε): 430 (1500), 328 (26300), 317 nm (22430 mol^{-1} dm^3 cm^{-1}); MALDI-TOF *m/z*: 1342.2 [M^+].

Compound 11: ^{1}H NMR ($CDCl_3$, 600 MHz): $\delta = 7.60$ (br, 2H, aromatic-H), 7.28 (d, 2H, $J = 8.2$ Hz, aromatic-H), 4.96 (d, 1H, $J = 9.2$ Hz, CH_2 pyrrolidine), 4.86 (d, 1H, $J = 9.2$ Hz, CH pyrrolidine), 4.23 (s, 1H, CH_2 pyrrolidine), 2.78 (s, 3H, aliphatic-CH_3), 2.08–2.03 (m, 12H, aliphatic -CH_2-), 1.21–1.16 ppm (m, 18H, aliphatic -CH_3); ^{13}C NMR ($CDCl_3$, 150 MHz): $\delta = 156.4$, 154.1, 153.6, 153.5, 147.3, 146.9, 146.5, 146.50, 146.2(2), 146.0(2), 145.8, 145.6, 145.5, 145.3, 144.8, 144.7, 144.4, 143.2, 142.7, 142.6, 142.3(2), 142.2, 142.1(3), 142.0, 141.9, 141.7, 141.6, 140.3, 140.2, 139.9, 139.7, 136.9, 136.6, 135.9, 135.8, 133.9, 131.2, 129.1, 128.8, 101.3, 100.3, 83.6, 70.1, 69.1, 40.1, 31.0, 29.8, 14.6, 14.5, 14.4, 8.1(2) ppm; ^{31}P NMR (243 MHz, $CDCl_3$): $\delta = 15.4$ ppm (t, $J_{Pt,P} = 2347.0$ Hz); FTIR (neat): $\tilde{\nu} = 2966$, 2934 (C–H), 2097 (alkyne), 1590, 1552, 1492, 1453, 1275, 1208, 1158, 1012, 830, 770, 693, 616, 527 cm^{-1}; FTIR (neat): $\tilde{\nu} = 2962$, 2776 (C–H), 2210 (alkyne), 1589, 1493, 1311, 1034, 863, 696, 523 cm^{-1}; UV/Vis (CH_2Cl_2): λ_{max} (ε): 430 (1357), 327 (25600), 318 nm (21780 mol^{-1} dm^3 cm^{-1}); MALDI-TOF *m/z*: 1342.2 [M^+].

TPA–*trans*-Pt–C_{60} (1): First CS_2 was used as eluent in order to remove unreacted C_{60} and then toluene, 35% yield; ^{1}H NMR ($CDCl_3$, 600 MHz): $\delta = 7.61$ (br s, 2H, aromatic-H), 7.30 (d, 2H, $J = 8.2$ Hz, aromatic-H), 7.21–7.19 (m, 4H, TPA-aromatic), 7.13 (d, 2H, $J = 8.2$ Hz, TPA), 7.06–7.04 (m, 4H, TPA), 6.97–6.95 (m, 2H, TPA), 6.90 (d, 2H, $J = 8.2$ Hz, TPA), 4.95 (d, 1H, $J = 9.2$ Hz, CH_2 pyrrolidine), 4.86 (d, 1H, $J = 9.2$ Hz, CH pyrrolidine), 4.22 (s, 1H, CH_2 pyrrolidine), 2.78 (s, 3H, aliphatic-CH_3), 2.21–2.14 (m, 12H, aliphatic -CH_2-), 1.21–1.13 ppm (m, 18H, aliphatic -CH_3); ^{13}C NMR ($CDCl_3$, 150 MHz): $\delta = 156.4$, 154.2, 153.7, 153.6, 147.8, 147.4, 147.3, 146.9, 146.6, 146.5, 146.4, 146.3(2), 146.2, 146.1, 146.0(2), 145.8, 145.6, 145.5(2), 145.4, 145.3(3), 145.2,(2), 144.9, 144.8, 144.7, 143.2, 143.0, 142.7, 142.6(2), 142.3(2), 142.2, 142.1, 142.0, 141.9, 141.7, 141.6, 140.2, 140.1, 139.9, 139.7, 136.8, 136.6, 135.8, 133.6, 131.7, 131.3, 129.2, 124.0, 133.5, 109.2, 109.0(2), 83.7, 70.1, 69.1, 40.1, 16.5, 16.4, 16.3, 8.5 ppm; ^{31}P NMR (243 MHz, $CDCl_3$): $\delta = 11.5$ ppm (t, $J_{Pt,P} = 2400.0$ Hz); FTIR (neat): $\tilde{\nu} = 3026$, 2926, 2774 (C–H), 2100 (alkyne), 1589, 1493, 1375, 1280, 1213, 1175, 1034, 828, 752, 696, 618 cm^{-1}; UV/Vis (CH_2Cl_2): λ_{max} (ε): 430 (1800), 356 (29900), 332 nm (28290 mol^{-1} dm^3 cm^{-1}); MALDI-TOF *m/z*: 1575 [M^+]; elemental analysis calcd (%) for $C_{103}H_{54}N_2P_2Pt$: C 78.47, H 3.45, N 1.80; found: C 78.48, H 3.80, N 1.79.

TPA–*cis*-Pt–C_{60} (2): First CS_2 was used as eluent in order to remove unreacted C_{60} and then toluene, 32% yield; ^{1}H NMR ($CDCl_3$, 600 MHz): $\delta = 7.61$ (br, 2H, aromatic-H), 7.30 (d, 2H, $J = 8.2$ Hz, aromatic-H), 7.21–7.19 (m, 4H, TPA), 7.13 (d, 2H, $J = 8.2$ Hz, TPA-aromatic), 7.06–7.04 (m, 4H, TPA), 6.97–6.95 (m, 2H, TPA), 6.90 (d, 2H, $J = 8.2$ Hz, TPA), 4.96 (d, 1H, $J = 9.2$ Hz, CH_2 pyrrolidine), 4.86 (d, 1H, $J = 9.2$ Hz, CH pyrrolidine), 4.22 (s, 1H, CH_2 pyrrolidine), 2.77 (s, 3H, aliphatic-CH_3), 2.19–2.14 (m, 12H, aliphatic -CH_2-), 1.22–1.12 ppm (m, 18H, aliphatic -CH_3); ^{13}C NMR ($CDCl_3$, 150 MHz): $\delta = 156.4$, 154.2, 153.7, 153.6, 147.8, 147.3, 146.6, 146.4, 146.3, 146.2, 146.1, 146.0, 145.9, 145.6(2), 145.5(2), 145.4, 145.3(3), 145.2(2), 145.0, 144.8, 144.7, 144.5, 143.2, 143.0, 142.7, 142.6(2), 142.3(2), 142.2(2), 142.1(2), 142.0, 141.9, 141.8, 141.6, 140.2, 140.1, 139, 9, 139.7, 136.8, 136.6, 135.8, 133.6, 131.7, 124.1, 124.0, 122.5, 109.4, 109.2, 109.0, 83.7, 70.1, 69.1, 40.0, 16.5, 16.3, 16.2, 8.4 ppm; ^{31}P NMR (243 MHz, $CDCl_3$): $\delta = 11.6$ ppm (t, $J_{Pt,P} = 2400.0$ Hz); FTIR (neat) $\tilde{\nu} = 3026$, 2962, 2770 (C–H), 2101(alkyne), 1589, 1493, 1375, 1281, 1175, 1034, 828, 754, 697, 617 cm^{-1}; UV/Vis (CH_2Cl_2), λ_{max} (ε): 430 (1730), 354 (27200), 331 nm (26100 mol^{-1} dm^3 cm^{-1}); MALDI-TOF *m/z*: 1575 [M^+]; elemental analysis calcd (%) for $C_{103}H_{54}N_2P_2Pt$: C 78.47, H 3.45, N 1.80; found: C 78.60, H 3.65, N 1.80.

Acknowledgements

L.E. thanks the Robert A. Welch Foundation for an endowed chair, grant #AH-0033, the US National Science Foundation, grant DMR-1205302 (PREM Program) and the Air Force Office of Scientific Research (grants FA9550-12-1-0053 and FA9550-12-1-0468) for the generous financial support. B.I. gratefully acknowledges financial support from COLCIENCIAS and Universidad del Valle.

Keywords: electron transfer · excited states · fullerenes · platinum(II) acetylide · triphenylamine

[1] J. Deisenhofer, H. Michel, *Angew. Chem.* **1989**, *101*, 872–892; *Angew. Chem. Int. Ed. Engl.* **1989**, *28*, 829–847.
[2] R. Huber, *Angew. Chem.* **1989**, *101*, 849–871; *Angew. Chem. Int. Ed. Engl.* **1989**, *28*, 848–869.
[3] M. R. Wasielewski, *Chem. Rev.* **1992**, *92*, 435.
[4] R. A. Marcus, N. Sutin, *Biochim. Biophys. Acta Rev. Bioenerg.* **1985**, *811*, 265.
[5] R. A. Wassel, C. B. Gorman, *Angew. Chem.* **2004**, *116*, 5230–5233; *Angew. Chem. Int. Ed.* **2004**, *43*, 5120–5123.
[6] J. M. Tour, *Acc. Chem. Res.* **2000**, *33*, 791.
[7] D. K. James, J. M. Tour, *Top. Curr. Chem.* **2005**, *257*, 33.
[8] E. A. Weiss, M. R. Wasielewski, M. A. Ratner, *Top. Curr. Chem.* **2005**, *257*, 103.
[9] R. C. Evans, P. Douglas, C. J. Winscom, *Coord. Chem. Rev.* **2006**, *250*, 2093.
[10] F. Guo, K. Ogawa, Y.-G. Kim, E. O. Danilov, F. N. Castellano, J. R. Reynolds, K. S. Schanze, *Phys. Chem. Chem. Phys.* **2007**, *9*, 2724.
[11] J. Mei, K. Ogawa, Y.-G. Kim, N. C. Heston, D. J. Arenas, Z. Nasrollahi, T. D. McCarley, D. B. Tanner, J. R. Reynolds, K. S. Schanze, *ACS Appl. Mater. Interfaces* **2009**, *1*, 150.
[12] E. E. Silverman, T. Cardolaccia, X. Zhao, K.-Y. Kim, K. Haskins-Glusac, K. S. Schanze, *Coord. Chem. Rev.* **2005**, *249*, 1491.
[13] F.-R. Dai, H.-M. Zhan, Q. Liu, Y.-Y. Fu, J.-H. Li, Q.-W. Wang, Z. Xie, L. Wang, F. Yan, W.-Y. Wong, *Chem. Eur. J.* **2011**, *17*, 1502.
[14] F. Guo, Y.-G. Kim, J. R. Reynolds, K. S. Schanze, *Chem. Commun.* **2006**, 1887.
[15] W.-Y. Wong, C.-L. Ho, *Acc. Chem. Res.* **2010**, *43*, 1246.
[16] W.-Y. Wong, X.-Z. Wang, Z. He, A. B. Djurišić, C.-T. Yip, K.-Y. Cheung, H. Wang, C. S. K. Mak, W.-K. Chan, *Nat. Mater.* **2007**, *6*, 521.
[17] W. Wu, X. Xu, H. Yang, J. Hua, X. Zhang, L. Zhang, Y. Long, H. Tian, *J. Mater. Chem.* **2011**, *21*, 10666.
[18] W. Wu, J. Zhang, H. Yang, B. Jin, Y. Hu, J. Hua, C. Jing, Y. Long, H. Tian, *J. Mater. Chem.* **2012**, *22*, 5382.
[19] F.-R. Dai, Y.-C. Chen, L.-F. Lai, W.-J. Wu, C.-H. Cui, G.-P. Tan, X.-Z. Wang, J.-T. Lin, H. Tian, W.-Y. Wong, *Chem. Asian J.* **2012**, *7*, 1426.

[20] F. Camerel, R. Ziessel, B. Donnio, C. Bourgogne, D. Guillon, M. Schmutz, C. Iacovita, J.-P. Bucher, *Angew. Chem.* **2007**, *119*, 2713 – 2716; *Angew. Chem. Int. Ed.* **2007**, *46*, 2659 – 2662.
[21] A. Y.-Y. Tam, K. M.-C. Wong, V. W.-W. Yam, *J. Am. Chem. Soc.* **2009**, *131*, 6253.
[22] X.-D. Xu, J. Zhang, L.-J. Chen, X.-L. Zhao, D.-X. Wang, H.-B. Yang, *Chem. Eur. J.* **2012**, *18*, 1659.
[23] T. Cardolaccia, Y. Li, K. S. Schanze, *J. Am. Chem. Soc.* **2008**, *130*, 2535.
[24] J. S. Wilson, A. S. Dhoot, A. J. A. B. Seeley, M. S. Khan, A. Köhler, R. H. Friend, *Nature* **2001**, *413*, 828.
[25] Y. Liu, S. Jiang, K. Glusac, D. H. Powell, D. F. Anderson, K. S. Schanze, *J. Am. Chem. Soc.* **2002**, *124*, 12412.
[26] F.-R. Dai, H.-M. Zhan, Q. Liu, Y.-Y. Fu, J.-H. Li, Q.-W. Wang, Z. Xie, L. Wang, F. Yan, W.-Y. Wong, *Chem. Eur. J.* **2012**, *18*, 1502.
[27] T. L. Schull, J. G. Kushmerick, C. H. Patterson, C. George, M. H. Moore, S. K. Pollack, R. Shashidhar, *J. Am. Chem. Soc.* **2003**, *125*, 3202.
[28] S. Chakraborty, T. J. Wadas, H. Hester, R. Schmehl, R. Eisenberg, *Inorg. Chem.* **2005**, *44*, 6865.
[29] S. Suzuki, R. Sugimura, M. Kozaki, K. Keyaki, K. Nozaki, N. Ikeda, K. Akiyama, K. Okada, *J. Am. Chem. Soc.* **2009**, *131*, 10374.
[30] Y.-J. Chen, S.-S. Chen, S.-S. Lo, T.-H. Huang, C.-C. Wu, G.-H. Lee, S.-M. Peng, C.-Y. Yeh, *Chem. Commun.* **2006**, 1015.
[31] A. J. Jimenez, M. L. Marcos, A. Hausmann, M. S. Rodriguez-Morgade, D. M. Guldi, T. Torres, *Chem. Eur. J.* **2011**, *17*, 14139.
[32] F. Nastasi, F. Puntoriero, S. Campagna, J.-H. Olivier, R. Ziessel, *Phys. Chem. Chem. Phys.* **2010**, *12*, 7392.
[33] J. R. Pinzón, D. C. Gasca, S. G. Sankaranarayanan, G. Bottari, T. Torres, D. M. Guldi, L. Echegoyen, *J. Am. Chem. Soc.* **2009**, *131*, 7727.
[34] A. Tigreros, V. Dhas, A. Ortiz, B. Insuasty, N. Martín, L. Echegoyen, *Sol. Energy Mater. Sol. Cells* **2014**, *121*, 61.
[35] Z. Ning, H. Tian, *Chem. Commun.* **2009**, 5483.
[36] A. Mishra, M. K. R. Fischer, P. Bauerle, *Angew. Chem.* **2009**, *121*, 2510 – 2536; *Angew. Chem. Int. Ed.* **2009**, *48*, 2474 – 2499.
[37] P. Qin, H. Zhu, T. Edvinsson, G. Boschloo, A. Hagfeldt, L. Sun, *J. Am. Chem. Soc.* **2008**, *130*, 8570.
[38] J.-H. Yum, D. P. Hagberg, S.-J. Moon, K. M. Karlsson, T. Marinado, L. Sun, A. Hagfeldt, M. K. Nazeeruddin, M. Gratzel, *Angew. Chem.* **2009**, *121*, 1604 – 1608; *Angew. Chem. Int. Ed.* **2009**, *48*, 1576 – 1580.
[39] P. Dutta, J. Kim, S. H. Eom, W.-H. Lee, I. N. Kang, S.-H. Lee, *ACS Appl. Mater. Interfaces* **2012**, *4*, 6669.
[40] A. Leliège, P. Blanchard, T. Rousseau, J. Roncali, *Org. Lett.* **2011**, *13*, 3098.
[41] H. Shang, H. Fan, Y. Liu, W. Hu, Y. Li, X. Zhan, *Adv. Mater.* **2011**, *23*, 1554.
[42] M. Zhu, J. Zou, S. Hu, C. Li, C. Yang, H. Wu, J. Qin, Y. Cao, *J. Mater. Chem.* **2011**, *21*, 361.
[43] J. Y. Kim, T. Yasuda, Y. S. Yang, C. Adachi, *Adv. Mater.* **2013**, *25*, 2666.
[44] A. A. Rachford, S. Goeb, F. N. Castellano, *J. Am. Chem. Soc.* **2008**, *130*, 2766.
[45] Q. Li, H. Guo, L. Ma, W. Wu, Y. Liu, J. Zhao, *J. Mater. Chem.* **2012**, *22*, 5319.
[46] P. J. Hay, W. R. Wadt, *J. Chem. Phys.* **1985**, *82*, 299.
[47] C. Liao, J. E. Yarnell, K. D. Glusac, K. S. Schanze, *J. Phys. Chem. B* **2010**, *114*, 14763.

Received: March 14, 2014
Published online on July 30, 2014